Journal of Structural Biology: X 10 (2024) 100110

Contents lists available at ScienceDirect

Journal of Structural Biology: X

journal homepage: www.sciencedirect.com/journal/journal-of-structural-biology-x

Conformational variability in the D2 loop of *Plasmodium* Apical Membrane antigen 1

Frederick A. Saul [a,g,1], Brigitte Vulliez-Le Normand [b,1], Alexander Boes [c,f], Holger Spiegel [c], Clemens H.M. Kocken [d], Bart W. Faber [d,*], Graham A. Bentley [e,g,*]

[a] Institut Pasteur, Université Paris Cité, CNRS UMR 3528, Plate-forme de Cristallographie C2RT, 75015 Paris, France
[b] Institut Pasteur, Université Paris Cité, CNRS UMR 3528, Unité de Microbiologie Structurale, 75015 Paris, France
[c] Fraunhofer Institute for Molecular Biology and Applied Ecology IME, Aachen, Germany
[d] Department of Parasitology, Biomedical Primate Research Centre, Rijswijk, the Netherlands
[e] Institut Pasteur, CNRS URA 2185, Unité d'Immunologie Structurale, 75015 Paris, France
[f] Current address: Leibniz-Institute for Interactive Materials, Aachen, Germany
[g] Current address: Institut Pasteur, Université Paris Cité, 75015 Paris, France

ARTICLE INFO

Keywords:
Apical Membrane Antigen 1
Domain 2 loop
Variable conformation
Plasmodium antigen
Malaria vaccine candidate

ABSTRACT

Apical Membrane Antigen 1 (AMA1) plays a vital role in the invasion of the host erythrocyte by the malaria parasite, *Plasmodium*. It is thus an important target for vaccine and anti-malaria therapeutic strategies that block the invasion process. AMA1, present on the surface of the parasite, interacts with RON2, a component of the parasite's rhoptry neck (RON) protein complex, which is transferred to the erythrocyte membrane during invasion. The D2 loop of AMA1 plays an essential role in invasion as it partially covers the RON2-binding site and must therefore be displaced for invasion to proceed. Several structural studies have shown that the D2 loop is very mobile, a property that is probably important for the function of AMA1. Here we present three crystal structures of AMA1 from *P. falciparum* (strains 3D7 and FVO) and *P. vivax* (strain Sal1), in which the D2 loop could be largely traced in the electron density maps. The D2 loop of PfAMA1-FVO and PvAMA1 (as a complex with a monoclonal antibody Fab) has a conformation previously noted in the *P. knowlesi* AMA1 structure. The D2 loop of PfAMA1-3D7, however, reveals a novel conformation. We analyse the conformational variability of the D2 loop in these structures, together with those previously reported. Three different conformations can be distinguished, all of which are highly helical and show some similarity in their secondary structure organisation. We discuss the significance of these observations in the light of the flexible nature of the D2 loop and its role in AMA1 function.

1. Introduction

Pathologies associated with malaria arise from infection of the host erythrocyte by the asexual blood-stage form, or merozoite, of the *Plasmodium* parasite. Host-cell invasion by the merozoite is a complex process involving interactions between several merozoite and erythrocyte surface proteins (Cowman, 2017). Among these is Apical Membrane Antigen 1 (AMA1), which is translocated from the microneme organelles to the merozoite surface prior to invasion (Narum, 1994). AMA1 binds to the rhoptry neck (RON) protein complex (Cao, 2009; Lamarque, 2011; Riglar, 2011), an association of parasite proteins stored in the rhoptries of the merozoite but transferred to the erythrocyte membrane at the moment of invasion. *Plasmodium* thus provides its own receptor for AMA1. AMA1 and the RON protein complex are present in the Moving Junction (MJ) (Riglar, 2011), a ring structure linking the merozoite and erythrocyte membranes in a tight association. As invasion progresses, the MJ moves over the entire merozoite surface to completely enclose the parasite within a parasitophorous vacuole inside the erythrocyte (Aikawa, 1978). AMA1 is essential for erythrocyte invasion as AMA1-specific antibodies (Deans, 1982; Coley, 2001; Coley, 2006; Collins, 2006), peptides (Harris, 2005; Wang, 2016; Akter, 2019) and small molecules (Srinivasan, 2013) can inhibit infection, and is thus an important target for vaccine and anti-malarial strategies.

AMA1 binds to the RON2 component of the RON protein complex

* Corresponding authors.
E-mail addresses: faber@bprc.nl (B.W. Faber), bentley.graham@orange.fr (G.A. Bentley).
[1] These authors contributed equally.

https://doi.org/10.1016/j.yjsbx.2024.100110
Received 7 July 2024; Received in revised form 5 September 2024; Accepted 6 September 2024
Available online 10 September 2024

Table 1
Crystallographic parameters and data collection statistics.

	PfAMA1-FVO	PfAMA1-3D7	PvAMA1-FabF8.1.1	FabF8.1.1
Synchrotron source	ESRF	SOLEIL	ESRF	ESRF
Beamline	ID23-2	PROXIMA 1	ID14-1	ID14-1
Space group	$P2_12_12_1$	P1	$P2_12_12$	$P2_1$
a, b, c (Å)	38.28, 94.22, 96.20	38.23, 62.06, 71.50	73.39, 214.68, 57.41	53.49, 61.52, 116.99
α, β, γ (°)	90, 90, 90	89.1, 89.9, 83.9	90, 90, 90	90, 97.5, 90
Resolution range (Å)	47.11–2.00 (2.05–2.00)*	47.06–2.10 (2.21–2.10)	73.39–3.05 (3.26–3.05)	46.02–2.10 (2.16–2.10)
Wavelength (Å)	0.8726	0.9786	0.9340	0.9340
Unique reflections	24,245 (1754)	37,352 (5400)	18,062 (3193)	41,875 (2478)
Completeness (%)	99.8 (99.8)	97.9 (96.8)	99.9 (100.0)	94.8 (69.0)
Multiplicity	3.6 (3.6)	2.0 (2.0)	7.1 (7.2)	3.8 (3.6)
Rmerge	0.128 (1.012)	0.199 (0.872)	0.167 (1.203)	0.139 (0.654)
Rpim	0.078 (0.615)	0.179 (0.795)	0.067 (0.480)	0.083 (0.399)
< I/σ(I) >	8.1 (1.3)	4.3 (2.1)	11.8 (1.7)	7.4 (1.9)
CC(1/2)	0.994 (0.491)	0.902 (0.215)	0.996 (0.316)	0.993 (0.507)

*Values in parentheses are for the high resolution shell.

Table 2
Refinement statistics.

	PfAMA1-FVO	PfAMA1-3D7	PvAMA1-FabF8.1.1	FabF8.1.1
Resolution (Å)	47.11 – 2.00 (2.05–2.00)*	46.37 – 2.10 (2.15–2.10)	69.54 – 3.05 (3.13–3.05)	42.24 – 2.10 (2.15–2.10)
No. reflections	22,895 (1590)	35,400 (2560)	17,069 (1229)	40,631 (2137)
R-value (work set)	0.177 (0.294)	0.207 (0.273)	0.221 (0.381)	0.200 (0.307)
Rfree (5 % of data)	0.219 (331)	0.256 (0.317)	0.292 (0.386)	0.255 (0.342)
Protein atoms	2621	4780	6293	6344
Solvent atoms	258	322	0	439
rms deviations				
bond length (Å)	0.01	0.01	0.02	0.01
bond angles (°)	1.47	1.73	1.65	1.07
Ramachandran:				
favoured	96 %	97 %	91 %	97 %
allowed	4 %	3 %	8 %	3 %
outlier	0 %	0 %	1 %	0 %
Protein Databank (PDB) entry	9EVN	9EVO	8REK	8REL

*Values in parentheses are for the high resolution shell.

(Cao, 2009; Srinivasan, 2011; Hossain, 2012), which also includes the proteins RON4 and RON5 in *Plasmodium* species. Studies have confirmed that AMA1 targets the extracellular region between the putative second and third transmembrane regions of RON2 (Hossain, 2012): the crystal structures of PfAMA1 in complex with the peptide segment Met2020-Leu2058 of PfRON2 (Vulliez-Le Normand, 2012), and of PvAMA1 in complex with the peptide segment Met2034-Leu2072 of PvRON2 (Vulliez-Le Normand, 2017) have been determined at high resolution. In addition, binding studies reveal a high affinity of these peptide ligands for AMA1 (~10 to 200 nM) (Vulliez-Le Normand, 2017). The crystal structures show that RON2 binds to the hydrophobic groove and an adjacent region that becomes accessible to the receptor after displacement of the Domain 2 (D2) loop of AMA1.

The D2 loop is a flexible region of Domain 2 located between helix α7 and β-strand β15 (Chesne-Seck, 2005; Delgadillo, 2016). The central region of 37 residues is particularly mobile (residues 351 to 387 in PfAMA1 and residues 296 to 332 in PvAMA1) and in our discussion we refer to this polypeptide segment as the D2 loop. Evidence for mobility comes mainly from crystal structure studies (Pizarro, 2005; Bai, 2005; Vulliez-Le Normand. 2012, 2015): the D2 loop exhibits high temperature factors and the loop has not been completely traced in any of the structures solved to date. Consistent with the numerous crystal structure results, molecular dynamics and NMR studies show a significant mobility, particularly in the N- and C-terminal extremities of the D2 loop (Lim, 2014). In crystal structures where the D2 loop has been largely defined, two principal conformations have been distinguished: Conformation A, first found in PfAMA1-3D7 (PDB entry 1Z40) (Bai, 2005) and Conformation B, present in PkAMA1 (PDB entries 4UV6 and 4UAO) (Vulliez-Le Normand, 2015). These two conformations are distinct from each other within the polypeptide segment 351–387 of PfAMA1 and the equivalent segment 296–332 of PkAMA1. However, both conformations partially occupy the RON2 binding site and must therefore be displaced by RON2 upon binding. Indeed, this segment is not visible in the structures of AMA1-RON2 complexes (PfAMA1-RON2 (PDB entry 3ZWZ), PvAMA1-RON2 (PDB entry 5NQG)), which is indicative of high mobility. Recent kinetic data suggest that association with RON2 is a 2-step process and that the D2 loop stabilises the AMA1-RON2 complex by lowering the dissociation rate in comparison to a PfAMA1 construct bearing a significantly truncated loop (Delgadillo, 2016).

We describe here the crystal structures of PfAMA1 from the FVO and 3D7 strains, and PvAMA1 (Sal1 strain) in complex with the Fab fragment from a specific monoclonal antibody (mAb). In each case, the D2 loop has been traced over a significant length of the polypeptide segment, allowing comparison between these three AMA1 structures and with those previously published. The D2 loop conformation in PfAMA1-FVO and the PvAMA1-Fab complex closely resembles that previously found in PkAMA1 (Vulliez-Le Normand, 2015) (Conformation B). By contrast, the D2 loop conformation in the PfAMA1-3D7 structure that we have determined differs from that previously reported for the same strain (Bai, 2005) (Conformation A, PDB entry 1Z40) and from Conformation B. It does, nonetheless, show some similarity to the D2 loop traced in PfAMA1-FVO complexed with a spin-labelled peptide (PDB entry 6N87) (Akter, 2019); we designate this third conformation as Conformation C. We discuss the implications of these discreet conformations in the light of the intrinsic mobility of this functionally important region of AMA1.

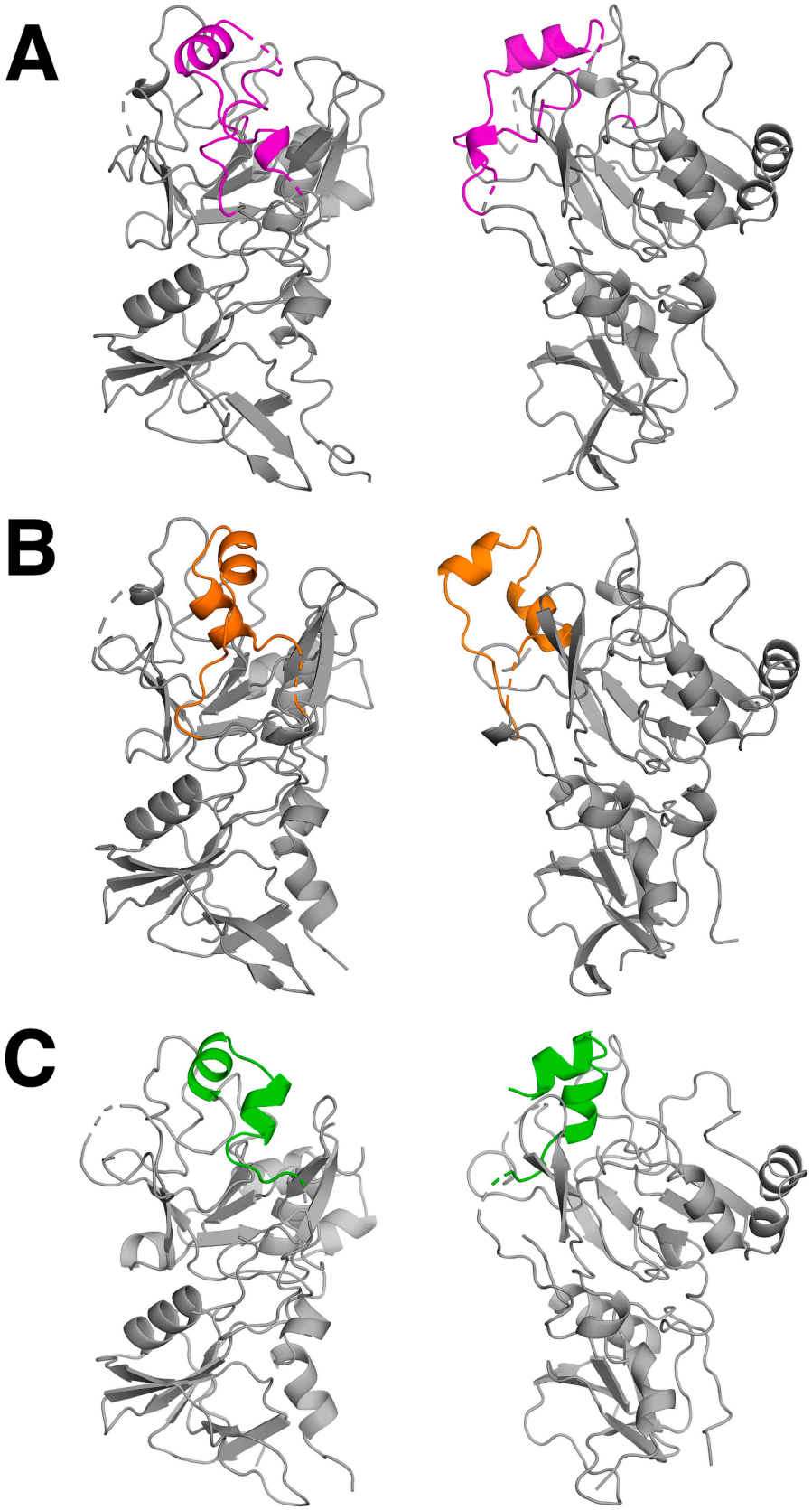

Fig. 1. Comparison of the D2 loop conformation in PfAMA1 from the FVO and 3D7 strains, and PvAMA1 strain Sal1. For each structure, two views related by a 90° rotation about a vertical axis are shown from the same perspective in ribbon representation, with Domains 1 and 2 of the AMA1 core in grey. **A** Structure of PfAMA1-FVO with the D2 loop shown in magenta. **B** Structure of PfAMA1-3D7 with the D2 loop shown in orange (molecule A). **C** Domains 1 and 2 of PvAMA1 with the D2 loop shown in green.

2. Results and discussion

2.1. General presentation of the crystallographic data and results

Crystallographic parameters and data processing statistics are summarised in Table 1; refinement statistics are reported in Table 2 for the four crystal structures.

2.2. General description of the AMA1 structures

(i) PfAMA1-FVO. The structure of the recombinant PfAMA1-FVO, comprising Domains 1 and 2 of the extracellular region and containing one molecule in the asymmetric unit, was refined at 2.0 Å resolution. The polypeptide chain was traced from Glu102 to Phe441 with gaps between residues Cys263 and Ser272, Asn369 and Asp373 (in the D2 loop), and Phe385 and Arg389 (D2 loop) (Fig. 1A).

(ii) PfAMA1-3D7. Domains 1 and 2 of the recombinant PfAMA1-3D7 crystallised in the space group P1 with two independent molecules in the unit cell; it thus differs from the previously published crystal structure of this strain, which crystallised in space group $P3_1$ (PDB entry 1Z40) (Bai, 2005). The structure was refined at 2.1 Å resolution; molecule A was traced from residues Gly107 to Pro442 with gaps between residues Lys265 and Ser272, and Phe379 and Ala387 (in the D2 loop) while molecule B was traced from Asn108 to Asn439, with gaps between Thr171 and Gln174, Asp229 and Ser232, Ala264 and Met273, and Tyr353 and Asp388 (D2 loop) (Fig. 1B). Thus, while the D2 loop of molecule A was entirely traced except for a seven-residue gap, that of molecule B was too disordered to be modelled. Although the crystals were soaked with the invasion inhibitory molecule B43 (7-Cyclopentyl-5-(4-phenoxy)phenyl-7H-pyrrolo[2,3-d]pyrimidin-4-ylamine, see sec. 4.4 for details) prior to mounting, no evidence for its presence was found in the electron density maps.

(iii) PvAMA1-FabF8.1.1 complex. The structure of PvAMA1 in complex with the Fab fragment of the specific mAb F8.1.1 was refined at 3.05 Å resolution (Fig. 2). The recombinant PvAMA1 protein, comprising the N-terminal segment and Domains 1 to 3 of the extracellular region of the antigen, was traced from residues Thr44 to Tyr474, with gaps between Val170 and Ser177, Asp211 and Ala217, Gln294 and Lys307 (D2 loop), and Val327 and Asp333 (D2 loop), and between residues Ser403 and Ser410 in Domain 3. Domains 1 and 2 of PvAMA1 are compared in Fig. 1C with those of PfAMA1-FVO and PfAMA1-3D7.

The epitope recognised by mAb F8.1.1 is composed of 14 Domain 3 residues, which include Cys432 and Cys434, belonging to the cystine knot (disulphide bridges Cys432-Cys449 and Cys434-Cys451) (Fig. 2). The V_H domain makes 76 interatomic contacts < 3.8 Å with PvAMA1, including 16 polar contacts, while the V_L domain makes 23 contacts, including 2H-bonds. The free FabF8.1.1, which contains two molecules in the asymmetric unit, was refined at 2.1 Å resolution. The significantly higher resolution of the free Fab structure aided the model building and refinement of this component in the complex.

2.3. Structural comparison of the D2 loop in different Plasmodium AMA1 homologues

In the three *Plasmodium* AMA1 structures we report here, the D2 loop could be traced in the electron density maps over a significant length in each case. The D2 loops of PfAMA1-FVO and PvAMA1 are similar in structure to that of PkAMA1 (PDB entries 4UV6 and 4UVO) (Vulliez-Le Normand, 2015) and thus belong to Conformation B (Fig. 3). For the PfAMA1-3D7 structure, however, the D2 loop conformation differs from Conformations A and B (Fig. 4) but shows some relationship to that found in PfAMA1-FVO in complex with a spin-labelled peptide (PDB entry 6N87), (Akter, 2019); we designate this D2 loop structure as Conformation C.

Although structurally distinct, Conformations A, B and C show a propensity to be helical. They contain either one or two α-helices that we designate as D2α1 and D2α2, depending on their position in the sequence (Fig. 5). D2α1 is present in all three conformations but its 3-D relationship to the AMA1 core differs in each conformation class. For example, while D2α1 makes contacts exclusively with the AMA1 core in Conformations A and B, this helix makes only intermolecular contacts in the two crystal structures where the D2 loop adopts Conformation C (PDB entries 9EVN (this study) and 6N87) and is thus strongly influenced by the lattice environment. Although D2α2 is absent in Conformation A, it is present in Conformations B and C (Fig. 5) and is stabilised exclusively by intramolecular contacts with the AMA1 core; however, its 3D disposition with respect to the core structure differs between these two conformations (Fig. 4).

For the PfAMA1-FVO structure reported in this study, the D2 loop (Conformation B) was traced from residues Ala351 to Phe385, with gaps 370–372 and 386–388. The D2α1 helix is present (Tyr360-Phe367) but the region where D2α2 is expected is not strictly α-helical. Here, the electron density indicates some conformational mobility and was difficult to model but the dihedral angles fall within the helical region of the Ramachandran plot; this is the only Conformation B structure where a strictly α-helical D2α2 is absent; however, the main chain closely follows

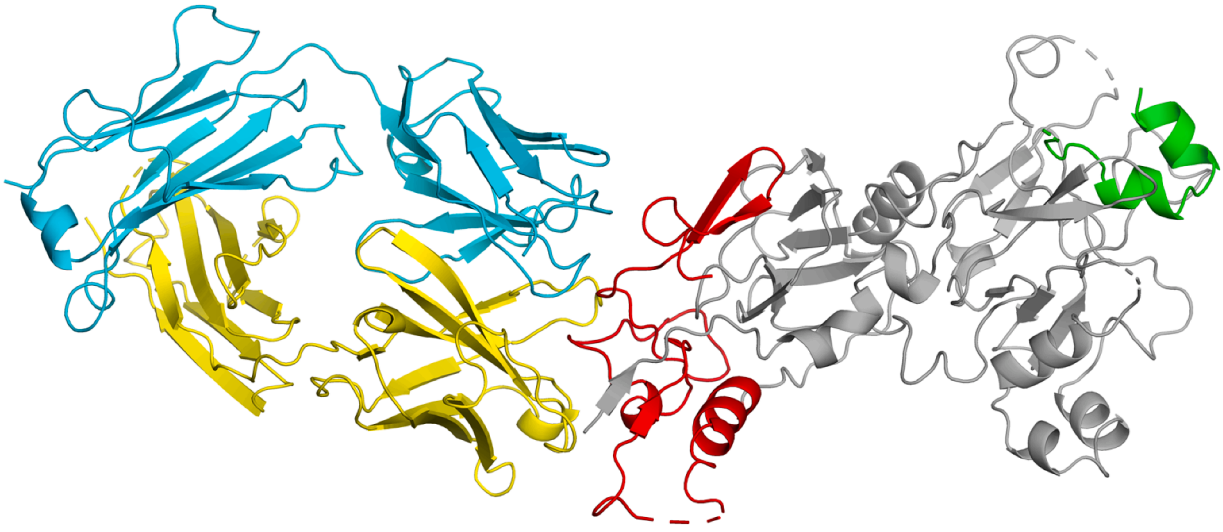

Fig. 2. Structure of PvAMA1 in complex with FabF8.1.1 shown in ribbon representation. Domains 1 and 2 of the AMA1 core are shown in grey and the D2 loop is shown in green; Domain 3 is shown in red. The heavy and light chains of FabF8.1.1 are shown in yellow and cyan, respectively.

Fig. 3. Comparison of the D2 loop in Conformation B from PfAMA1-FVO, PvAMA1 and PkAMA1. The structures are shown in ribbon representation with PfAMA1-FVO in magenta, PvAMA1 in green and PkAMA1 (PDB entry 4UV6) in yellow. The complete structures of the three AMA1 molecules were superimposed to produce this comparison. Dashed regions of the polypeptide correspond to segments that could not be traced in the electron density maps but were interpolated by the program PyMol.

the trace of the other examples, as can be seen in Fig. 3. An α-helix occurs in the region Thr382-Ala384 of PfAMA1-FVO but is only 3 residues in length and is not found in other structures (Figs. 3, 5). For PvAMA1 in the FabF8.1.1 complex, the D2 loop (Conformation B, residues Ala296 to Arg332) was traced except for gaps 296–306, and 328–332. Here, the loop contains two α-helices: D2α1 (Ile308-Gln314) and D2α2 (Arg317-Ser322) (Fig. 5). The D2 loop conformations of both PfAMA1-FVO and PvAMA1 are similar to that of PkAMA1 (reference for Conformation B, PDB entries 4UV6 and 4UVO) **(**Fig. 3**)**, which has the two α-helices D2α1 (Asp304-Gln314) and D2α1 (Asn316-Ala323). (PvAMA1 and PkAMA1 have identical residue numbering for the first two domains.) Although the helical residue limits of PfAMA1-FVO, PvAMA1 and PkAMA1 do not perfectly align, their overlap is nonetheless significant (Fig. 5).

The D2 loop of the PfAMA1-3D7 structure (Conformation C) that we have determined was completely traced in molecule A except for the seven-residue gap 380–386; however, it was completely disordered in the region 354–387 of molecule B (the second molecule of the asymmetric unit). The D2 loop of molecule A contains the two α-helices D2α1 (Asp359-Lys364) and D2α2 (Asn369-Lys376), which closely align in sequence with the Conformation B helices of PkAMA1 (Fig. 5) but not in 3-dimensional structure (Fig. 4).

2.4. *Influence of crystal packing on the D2 loop conformation*

In all reported AMA1 crystal structures where the D2 loop could be traced over a significant length, the loop makes contacts with symmetry-related molecules. This suggests that stabilisation by the crystal environment could be important in capturing the D2 loop in a conformation that is sufficiently ordered to be followed in the electron density maps. We considered this question further by examining the potential for intermolecular contacts and the possibility of steric hindrance of Conformations A, B and C by the crystal lattice environments of all *Plasmodium* AMA1 structures published to date, including the structures reported here. Accordingly, we used PfAMA1-3D7 (1Z40), PkAMA1 (4UV6) and PfAMA1-3D7 (this study, 9EVO) as templates for Conformations A, B and C, respectively, to address this question *via* the following qualitative analysis. The AMA1 core of each of these three reference structures was superimposed in turn upon that of each crystal structure and the environment of the D2 loop was inspected. (The D2 loop was not included in the superposition calculation.) AMA1 structures in complex with the RON2 peptide (PDB entries 3ZWZ, 5NQG) were not included in this analysis since the D2 loop is displaced by the ligand and could not be traced in any of these studies. The results from a total of 14 *Plasmodium* AMA1 crystal structures are summarised in Fig. 6. This ensemble gave 18 independent AMA1 molecular structures as four crystal structures had two (independent) molecules in the asymmetric unit. The D2 loop could be traced in 13 of these individual AMA1 molecules: six with Conformation A (one of which was very partial: PDB entry 4R1B), five with conformation B and two with Conformation C.

In many cases, steric hindrance by neighbouring molecules in the crystal lattice plays a clear role in excluding one or more of the Conformations A, B and C. For example, in the two PvAMA1 crystal structures, where no structure for the loop could be traced (1W8K, 1W81), all three conformations clashed with symmetry-related molecules. In the crystal environment of PvAMA1 in complex with the FabF8.1.1 reported here, where the D2 loop adopts the Conformation B, steric clashes with other molecules in the lattice environment occurred with Conformations A and C. Similarly, for PfAMA1-3D7 (1Z40), where the D2 loop adopts the Conformation A in both molecules of the asymmetric unit, steric clashes occurred with Conformations B and C.

In other examples, a D2 loop template conformation appeared compatible with the lattice environment (i.e., no clear steric clashes) but did not correspond to the structure observed in the crystal; this occurred 12 times (see Fig. 6). Favourable intermolecular contacts (complementary polar and apolar interactions) are important in selecting and stabilising the conformation of the D2 loop; within a given crystal lattice, these need to be sufficient to stably sequester a conformation. In the structure of PfAMA1-3D7 (this study, PDB entry 9EVO), where the D2 loop is in Conformation C, there were no clear stabilising contacts evident for Conformations A and B. In this crystal structure, moreover, there are two molecules in the asymmetric unit; for the second molecule, which showed no ordered D2 loop structure, none of the three conformations showed potential stabilising contacts with neighbouring molecules in the lattice.

The importance of crystal contacts is particularly evident in the comparison of the two structures PfAMA1-3D7 (PDB entry 9EVO) and PfAMA1-FVO (PDB entry 6N87) where the D2 loop is in Conformation C (Fig. 7). The D2α2 helices of these two structures superimpose very closely and make contacts with the AMA1 core only (i.e., are not involved in intermolecular contacts in the crystal lattice). By contrast, the D2α1 helices do not superimpose and make contacts exclusively with symmetry-related molecules in the crystal, which are different in these two structures. Intermolecular contacts thus appear important in modulating the structure of this intrinsically mobile region of AMA1. In Conformations A and B, moreover, D2α1 makes important contacts with the AMA1 core, suggesting that Conformation C is less stable in the

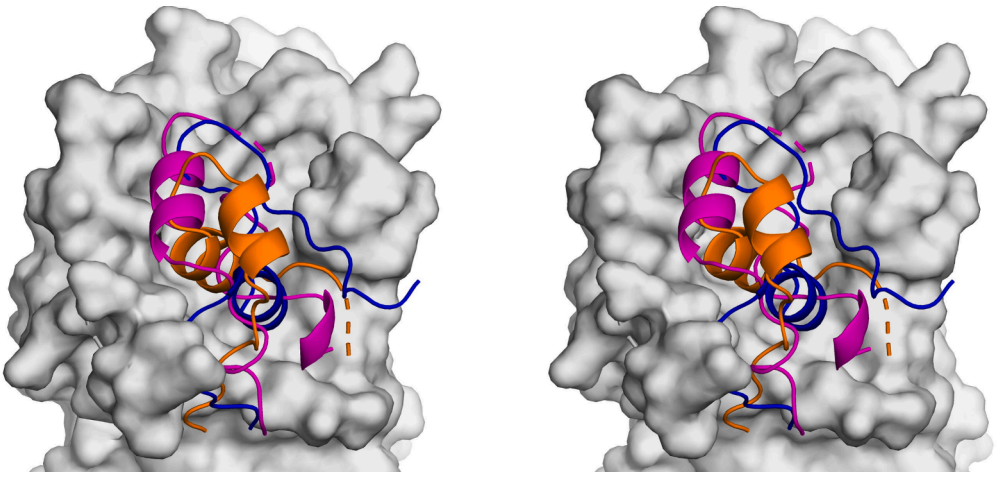

Fig. 4. A stereo view comparing Conformations A, B and C in PfAMA1. The D2 loops of PfAMA1-3D7 (Conformation A, PDB entry 1Z40, shown in blue), PfAMA1-FVO (Conformation B, this study, PDB entry 9EVN, magenta) and that of PfAMA1-3D7 (Conformation C, this study, PDB entry 9EVO, orange) are compared in ribbon presentation after superposition of the core AMA1 structures. They are shown against the surface presentation of the PfAMA1-FVO core, shown in grey. Dashed regions of the polypeptide correspond to segments that could not be traced in the electron density maps but were interpolated by the program PyMol.

```
PfAMA1     seq no.          350  355  360  365  370  375  380  385
Pv/PkAMA1 seq no.           295  300  305  310  315  320  325  330
                             +    +    +    +    +    +    +    +
α-helix assignment.                      D2α1      D2α2

PfAMA1-3D7 (1Z40)    Conf A  *******HHHHHHHH*****************_____
PfAMA1-FVO (9EVN)    Conf B  *********HHHHHHHH**___*********HHH___
PvAMA1     (8REK)    Conf B  ___________*HHHHHHH**HHHHHH****______
PkAMA1     (4UV6)    Conf B  ********HHHHHHHHHHH*HHHHHHHH****____*
PfAMA1-3D7 (9EVO)    Conf C  ********HHHHHH****HHHHHHHH***_______*
PfAMA1-FVO (6N87)    Conf C  ***_____*HHHHHH**HHHHHHHHHHHH**____*
```

Fig. 5. Secondary structure of the D2 loop in different conformations. The secondary structure of the D2 loop Conformations A, B and C are compared using the crystal structures PfAMA1-3D7 (PDB entry 1Z40), PfAMA1-FVO (9EVN), PvAMA1 (8REK), PkAMA1 (4UV6), PfAMA1-3D7 (9EVO) and PfAMA1-FVO (6N87). Structures and PDB entries that were not determined in the present study are indicated in red. Lines 1 and 2 indicate the aligned residue numbering for the *P. falciparum*, *P. vivax* and *P. knowlesi* homologues. Line 3 gives the position of helices D2α1 and D2α2. For each structure, residues in the α-helical conformation are indicated by 'H', other conformations by '*' and untraced residues by '_'. The α-helical conformation was assigned using the program PyMol.

isolated molecule.

2.5. D2 loop structures form a restricted repertoire of conformations

Although the above analysis implies that the D2 loop conformation requires stabilisation *via* intermolecular contacts in order to be observed in a crystal structure, comparison between the different *Plasmodium* AMA1 crystal structures suggests that its conformation is limited to a small repertoire of distinct structures. Conformation A, the first D2 loop structure to be reported, was observed in the two independent molecules in the crystal form of PfAMA1-3D7 from the PDB entry 1Z40. The same conformation was later found in PfAMA1-3D7 in complex with antibody fragments (Henderson, 2007; Coley, 2007) (PDB entries 2Q8A and 2Z8V) and in one other crystal form of PfAMA1-3D7 (PDB entry 4R1B) (Lim, 2014), although in the latter structure the length of the traced D2 loop was very partial. Conformation B was first reported in the crystal structures of PkAMA1 in the free form (with two molecules in the asymmetric unit) and as an antibody-bound form (Vulliez-Le Normand, 2015). Since the D2 loops of these two PkAMA1 crystal structures closely superimposed, and noting that the antibody made extensive contacts with the loop, Conformation B may represent the lowest energy structure in this *Plasmodium* species as it forms part of a conformational B-cell epitope of the native antigen. Indeed, the antibody prevents displacement of the D2 loop as well as blocking the exposed region of the RON2-binding site, thus completely precluding engagement with the receptor. Moreover, the PfAMA1-FVO and PvAMA1 structures that we report in the present study show that Conformation B occurs in different species, indicating that it is more widely implicated in the *Plasmodium* AMA1 structure. Finally, we have described the Conformation C of the D2 loop in PfAMA1-3D7. Our analysis of the effects of molecular packing in the diverse crystal forms of different *Plasmodium* AMA1 molecules shows that the steric environment within the lattice has a determining influence in selecting the particular D2 loop conformation. The free energy differences between the three conformations are probably small and

AMA1 crystal structure	Conf A	Conf B	Conf C
PfAMA1-FVO 9EVN, 2.00 Å			
PfAMA1-3D7 9EVO, 2.10 Å (Mol. A)			
PfAMA1-3D7 9EVO, 2.10 Å (Mol. B)			
PvAMA1 8REK, 3.05 Å			
PfAMA1-3D7 1Z40, 1.90 Å (Mol. A)			
PfAMA1-3D7 1Z40, 1.90 Å (Mol. Z)			
PfAMA1-3D7 2Q8A, 2.40 Å			
PfAMA1-3D7 2Z8V, 2.35 Å (Mol. A)			
PfAMA1-3D7 2Z8V, 2.35 Å (Mol. B)			
PfAMA1-3D7 4R1B, 1.60 Å			
PfAMA1-3D7 4R1C, 2.00 Å			
PfAMA1-FVO 6N87, 1.59 Å			
PfAMA1-FVO 4R1A, 2.00 Å			
PkAMA1 4UV6, 2.45 Å (Mol. A)			
PkAMA1 4UV6, 2.45 Å (Mol. B)			
PkAMA1 4UAO, 3.10 Å			
PvAMA1 1W8K, 1.80 Å			
PvAMA1 1W81, 2.01 Å			

Fig. 6. Influence of the lattice on the D2 loop conformation in *Plasmodium* AMA1 crystal structures. The first column gives the AMA1 structure with PDB entry and the resolution of the structural study; crystal structures with two molecules in the asymmetric unit are distinguished by the chain label in the PDB entry. The second, third and fourth columns show the effect of the crystal lattice on Conformations A, B and C, respectively: a green box indicates the observed conformation when the D2 loop could be traced; a yellow box indicates that the conformation is sterically hindered by the lattice; a blue box indicates that the conformation is sterically possible but was not observed. For clarity, structures for which the D2 loop was not traced are shaded in grey in the first column.

thus define local energy minima in the D2 loop structure. Thus, Conformations A, B and C are observed in different PfAMA1 structures (Fig. 4). All three conformations are significantly helical and have a very similar secondary structure organisation, which could facilitate transitions between them.

2.6. Implications of the D2 loop conformations for receptor binding

The D2 loop occupies one end of the receptor-binding site in all three conformations and must therefore be displaced in each case for complete binding of the RON2 ligand, as shown in Fig. 8. A comparison of solvent-inaccessible surfaces between the AMA1 core, on one hand, and the three D2 loop conformations or the RON2 ligand, on the other, is given in Table 3 for the *P. falciparum* homologue. These calculations show that Conformation B covers the largest surface of the binding site, Conformation A gives intermediate coverage, while Conformation C gives the least coverage. This suggests that Conformation B could be the most stable of the three, in line with our discussion on the D2 loop of PkAMA1 in section 2.5, which forms part of a conformational epitope recognised by an invasion-inhibitory antibody (Vulliez-Le Normand, 2015). Conformations A and C could be of intermediate and least stability, respectively, between the three D2 loop structures.

Structural and mutagenesis studies have revealed the presence of an arginine-specific binding pocket at the PfAMA1/PfRON2 interface that confers a fine specificity of the interaction for the *P. falciparum* species (Vulliez-Le Normand, 2012). This pocket is located at the extremity of the RON2-binding site that is distal to the D2 loop and which accommodates the side chain of Arg2041 of the ligand (Fig. 8). This pocket also accepts an arginine side chain from the peptide R1 (Vulliez-Le Normand, 2012) and antibodies 1F9 (Coley, 2007) and IgNAR (Henderson, 2007), which are invasion-inhibitory ligands for PfAMA1 that attach to the PfRON2-binding site. Access to the arginine-specific pocket is not blocked by Conformations A, B or C (Fig. 8) and thus a two-step model for the association of PfAMA1 and PfRON2, suggested by kinetic studies (Delgadillo, 2016), can be envisaged as an initial engagement of Arg2041 of PfRON2 to the accessible end of the binding site followed by the displacement of the D2 loop, freeing the remaining surface to complete the formation of the PfAMA1-PfRON2 complex. Arg2041 is close to the tip of a β-stranded cystine loop of PfRON2 and is thus well positioned to initiate contact with PfAMA1. A binding model for other plasmodial species could be different since residues homologous to Arg2041 are threonine or leucine.

3. Conclusions

Functional and structural data reveal an important role played by the D2 loop of AMA1 during invasion of the host erythrocyte by the *Plasmodium* merozoite. In crystal structures where the loop could be traced, it partially occupies the RON2-binding site and must therefore be displaced when AMA1 attaches to its receptor, as has been confirmed by structural studies of AMA1 in complex with RON2-based peptides (Vulliez-Le Normand, 2012). With the additional *Plasmodium* AMA1 structures described here, three distinct conformational forms of the D2 loop, Conformations A, B and C, can be identified. Conformation A has only been observed in PfAMA1 but in each case the lattice environments are different. Conformation B, however, has been found in the AMA1 crystal structures of three different *Plasmodium* species where they crystallise in distinct lattice environments. Conformations A and B may therefore be intrinsic to the *Plasmodium* AMA1 structure, occurring predominantly in solution where steric factors of the crystal lattice do not come into play. Conformation C, the third D2 loop structure, appears to be the least stable as it makes the lowest number of contacts with the AMA1 core. However, we cannot exclude the possibility that the three D2 loop conformations we have analysed here are representative of a restricted number of low energy structures that this region of AMA1 may adopt and between which may readily interchange. These observations

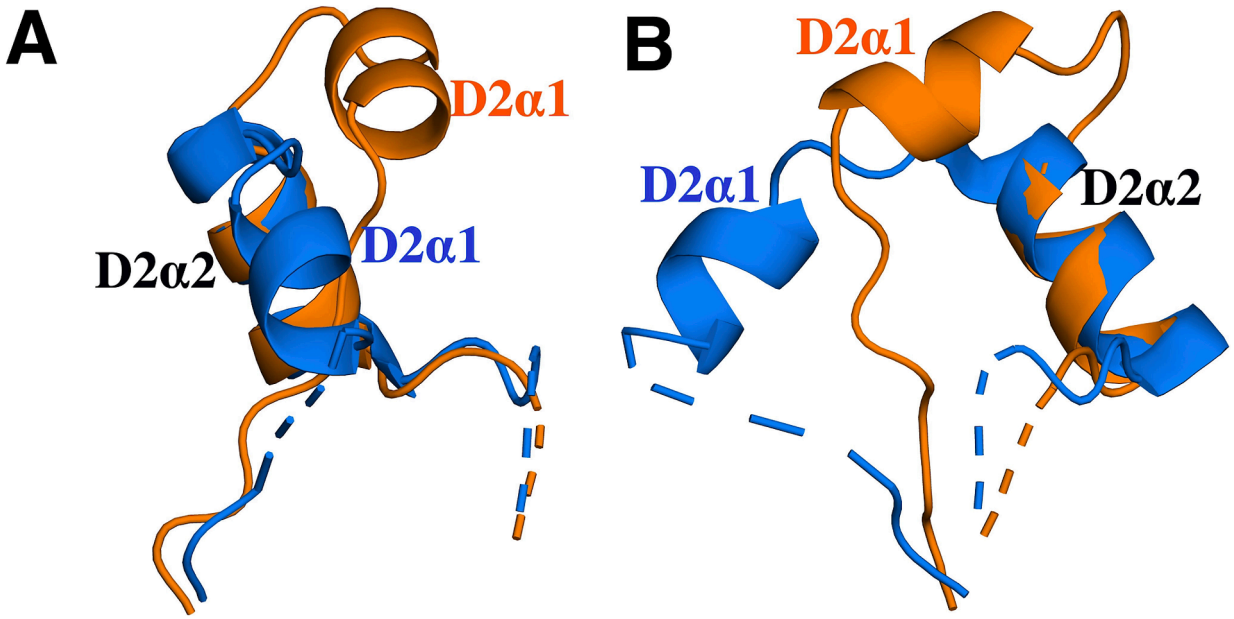

Fig. 7. Conformation C of the D2 loop. The D2 Loops of PfAMA1-3D7 (PDB entry 9EVO, molecule A) and PfAMA1-FVO (PDB entry 6N87) (Akter, 2019), which are in Conformation C, are compared in ribbon representation after superposition of the two structures. Two views are shown (**A**, **B**), which differ by a 90° rotation about a vertical axis. PfAMA1-3D7 is shown in orange and PfAMA1-FVO is shown in blue. Helix D2α1 is labelled in orange and blue for PfAMA1-3D7 (9EVO) and PfAMA1-FVO (6N87), respectively. Helices D2α2, which superimpose in the two structures, are labelled in black. Dashed regions of the polypeptide correspond to segments that could not be traced in the electron density maps but were interpolated by the program PyMol.

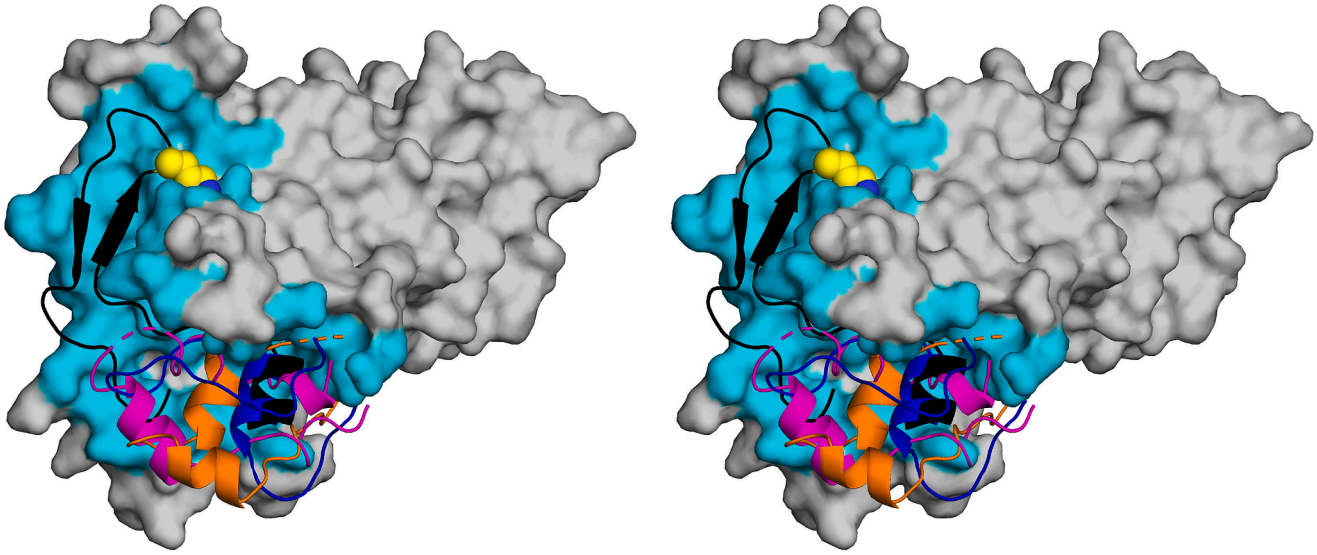

Fig. 8. Stereo view of the PfRON2 binding site on PfAMA1-3D7. The presentation of the PfAMA1-PfRON2sp peptide complex (Vulliez-Le Normand, 2012) (PDB entry 3ZW2) shows PfAMA1 in surface representation and the PfRON2sp peptide in ribbon representation (black). The solvent-inaccessible surface of PfAMA1 buried by PfRON2sp is shown in cyan; the remaining surface is in grey. Conformations A, B and C, coloured blue, magenta and orange, respectively (as in Fig. 5), are shown after superposition of PfAMA1 coordinates of PDB entries 1Z40, 9EVN and 9EVO, respectively, onto those of 3ZWZ. The critical side chain of residue Arg2041 of PfRON2 is shown as a space-filling atomic model (carbon in yellow, nitrogen in blue).

are of significance in understanding the dynamic behaviour of this functionally important region of AMA1.

4. Methods and Materials

4.1. Recombinant protein production

The recombinant PvAMA1-Sal1 protein, comprising Domains 1 to 3 (residues 43–487, followed by c-myc epitope and *hexa*-histidine tags, and with mutations Ser178 → Asn, Asn226 → Asp and Asn441 → Gln to remove potential N glycosylation sites), was produced in *Pichia pastoris* as described before (Vulliez-Le Normand, 2004). Recombinant PfAMA1-FVO, comprising Domains 1 to 2 (residues 106–442, preceded by Glu102-Ala103-Glu104-Phe105 arising from the cleavage site of a yeast protease and followed by the same C-terminal extension as PvAMA1) was expressed as described previously (Faber, 2007). The mutations Asn162 → Lys, Thr288 → Val, Ser373 → Asp, Asn422 → Asp and Ser423 → Lys were introduced to remove potential N-glycosylation sites. Recombinant PfAMA1-3D7, comprising Domains 1 to 2 (residues 97–442 with mutations Thr164 → Ala, Thr298 → Ala, Ser373 → Ala, Ser423 →

Table 3
Comparison of buried surfaces: D2 loop conformations and PfRON2. The solvent-inaccessible, or buried, surface between the core of PfAMA1 and the three D2 loop conformations or the PfRON2sp peptide were calculated using the program PISA (Krissinel and Henrick, 2007). Since the D2 loop is covalently linked to the PfAMA1 core, we removed two residues from both the N- and C-terminal extremities of the D2 loop (residues 351, 352, 386 and 387) if traced.

Structure (PDB entry)	Buried surface area (Å^2)
PfAMA1-3D7 Conformation A (1Z40)	1907
PfAMA1-FVO Conformation B (9EVN)	2298
PfAMA1-3D7 Conformation C (9EVO)	1438
PfAMA1-3D7/ PfRON2 complex (3ZWZ)	3167

Ala and Ser424 → Ala introduced to remove potential N-glycosylation sites) followed by the C-terminal *hexa*-histidine tag and the Ser-Glu-Lys-Asp-Glu-Leu ER-retrieval sequence, was produced by transient expression in *N. benthamiana* leaves as described before (Boes, 2015).

4.2. Production of monoclonal antibody and FabF8.1.1

The mAb F8.1.1 was obtained by immunization of BALB/c mice with the recombinant PvAMA1. The antibody (isotype IgG2b, κ) was precipitated from ascites fluid with ammonium sulphate and purified by ion–exchange chromatography (Mono Q). Fab fragments were produced by cleavage with papain (1:70, w/w protease to substrate) and purified on a DEAE-Sephacel column, followed by injection on a Mono Q ion-exchange column using a NaCl gradient to separate isoforms. The major isoform obtained was used for subsequent crystallisation trials.

4.3. Nucleotide sequencing of mAb F8.1.1

A total mRNA fraction was purified from 10^7 F8.1.1 hybridoma cells by guanidinium thiocyanate extraction and used as a substrate for cDNA synthesis by reverse transcription with an oligo(dT) primer. cDNA for V_H was amplified by PCR using primers V_H IIID (5′-GAA GTG CAG CTC GAG GAG TCT GGG GG-3′) and IgG1 (5′-GCA AGG CTT ACT AGT TGA AGA TTT GGG CTC AAC TTT CTT GTC GAC-3′) (G. Orsanoudakis and P. Lafaye, personal communication) while the light chain variable region (V_L) gene was amplified with the primers MuIgκV_L5′-G (mouse Ig-primer set, Novagen) and C_κ (5′-GCG CCG TCT AGA ATT AAC ACT CAT TCC TGT TGA A-3′) (Kang, 1991). The nucleic acid sequence was determined by Cogenics, France, using the resulting PCR products. Sequences were analysed using the program IMGT/V-Quest (Brochet, 2008; Giudicelli, 2011). An N-terminal pyroglutamate was found for the V_L chain and the terminal amino sequence was determined for the V_H chain as EVQLVE (Laboratoire de Microséquençage des Protéines, Institut Pasteur, Paris).

4.4. Crystallisation and diffraction measurements

All crystallisations were carried out by the vapour diffusion method using a hanging drop of protein solution sealed over a reservoir containing 1 ml of crystallisation buffer. Crystallisation boxes were left at 17 °C.

(i) Crystals of PfAMA1-FVO were obtained by mixing 1 µl of protein at 7.0 mg/ml concentration and 1 µl of reservoir buffer containing 35 % PEG 5000 monomethylether, 0.1 M Tris pH 8.5 and 0.2 M Li_2SO_4. Cryo-protecting buffer for PfAMA1-FVO crystals consisted of the crystallisation buffer mixed with glycerol (15 % v/v final concentration).

(ii) Crystals of PfAMA1-3D7 were obtained by mixing 1.2 µl of protein at 7.0 mg/ml concentration and 1.2 µl of reservoir buffer containing 12 % PEG 3350, 0.1 M Hepes pH 7 and 10 % propanol-2. Before mounting, a 20 mM solution of 7-Cyclopentyl-5-(4-phenoxy)phenyl-7H-pyrrolo[2,3-d]pyrimidin-4-ylamine (Sigma) (demonstrated as inhibiting the AMA1-RON2 interaction (Srinivasan, 2013) and referenced as B43 in the PDB) was prepared in DMSO and half diluted with the reservoir buffer; 1 µl of this mixture was then added to the drop containing the crystals, which were allowed to soak for 10 min before cryo-freezing. Cryo-protecting buffer for the crystals consisted of 10 % of a 20 mM solution of B43 and 90 % of the reservoir buffer with the PEG concentration increased to 20 % and supplemented with glycerol (10 % v/v final concentration).

(iii) PvAMA1 and FabF8.1.1 were mixed in a 1:1 stoichiometric ratio and left to incubate for 4 h at room temperature before mixing with crystallisation screening buffers. Crystals used for diffraction measurements were obtained by mixing 0.8 µl of the protein complex at 7.2 mg/ml concentration with 0.2 µl of 15 % 1,2,3 heptanetriol and 0.8 µl of reservoir buffer comprising 20 % PEG 2000 monomethylether and 0.1 M Tris pH 7. Cryo-protecting buffer for PvAMA1-FabF8.1.1 complex consisted of the crystallisation buffer mixed with glycerol (25 % v/v final concentration).

(iv) Crystals of FabF8.1.1 were obtained by mixing 1 µl of protein at 7.2 mg/ml concentration and 1 µl of reservoir containing 24 % PEG 4000, 80 mM sodium acetate pH 4.6 and 0.16 M ammonium acetate. Cryo-protecting buffer for FabF8.1.1 consisted of the crystallisation buffer, where PEG was increased to 30 %, mixed with glycerol (15 % v/v final concentration).

4.5. Diffraction measurements, data analysis and structure determination

Diffraction images were collected on beamlines at the ESRF, Grenoble, and SOLEIL, Saint Aubin (See Table 1 for details). Diffraction intensities were integrated using the program XDS (Kabsch, 2010) and data reduction calculations were carried out with programs from the CCP4 suite (Winn, 2011).

All structures were solved by molecular replacement using the program PHASER (McCoy, 2007). Search models were taken from PDB entry 1Z40, molecule A (PfAMA1-3D7), for the PfAMA1-FVO and PfAMA1-3D7 structures reported here. The coordinates of the PDB entry 6YHQ (FabF5.18.6) served as a search model for the free FabF8.1.1 structure. For the PvAMA1-FabF8.1.1 structure, the coordinates of PDB entry 1W8K (PvAMA1) and FabF8.1.1 were used to place the two components of the complex. Since the FabF8.1.1 structure was determined at 2.1 Å resolution, this facilitated the refinement of the complex where the diffraction data extended to only 3.05 Å. All structure refinements were made using the program REFMAC5 (Murshudov, 1997) and manual adjustments to the crystal structures were made with respect to the electron density maps using the graphics program COOT (Emsley, 2010). Structural figures were produced with the program PyMOL (The PyMOL Molecular Graphics System, Version 3.0 Schrödinger, LLC.).

CRediT authorship contribution statement

Frederick A. Saul: Writing – original draft, Investigation, Formal analysis. **Brigitte Vulliez-Le Normand:** Writing – original draft, Investigation, Formal analysis, Conceptualization. **Alexander Boes:** Writing – review & editing, Resources. **Holger Spiegel:** Writing – review & editing, Resources. **Clemens H.M. Kocken:** Writing – review & editing, Resources. **Bart W. Faber:** Writing – review & editing, Resources, Conceptualization. **Graham A. Bentley:** Conceptualization, Investigation, Formal analysis, Writing – original draft.

Declaration of competing interest

The authors declare that they have no known competing financial interests or personal relationships that could have appeared to influence the work reported in this paper.

Data availability

The atomic coordinates and structure factor data have been deposited in the Protein Data Bank with accession codes 9EVN (PfAMA1-FVO), 9EVO (PfAMA1-3D7), 8REK (PvAMA1-Fab8.1.1) and 8REL (Fab8.1.1). The V_H and V_L nucleotide sequences of F8.1.1 have been deposited in the GenBank with accession codes MN52086 and MN52087, respectively.

Acknowledgements

This work was supported by the Institut Pasteur, France, the Centre National de la Recherche Scientifique, France, the Biomedical Primate Research Centre, the Netherlands, and the Fraunhofer Institute for Molecular Biology and Applied Ecology, Germany. We acknowledge SOLEIL and ESRF for providing synchrotron radiation facilities and we thank the respective beamline staff for their assistance. We also thank the staff of the Crystallography Platform, Institut Pasteur, for technical assistance and access to computing facilities, and Marie-Madeleine Riottot for providing the monoclonal antibody F8.1.1.

References

Aikawa, M., et al., 1978. Erythrocyte entry by malarial parasites. A moving junction between erythrocyte and parasite. J. Cell Biol. 77, 72–82.
Akter, M., et al., 2019. Identification of the binding site of Apical Membrane Antigen 1 (AMA1) inhibitors using a paramagnetic Probe. Chem. Med. Chem. 14, 603–612.
Bai, T., et al., 2005. Structure of AMA1 from *Plasmodium falciparum* reveals a clustering of polymorphisms that surround a conserved hydrophobic pocket. Proc. Natl. Acad. Sci. u. s. a. 102, 12736–12741.
Boes, A., et al., 2015. Detailed functional characterization of glycosylated and nonglycosylated variants of malaria vaccine candidate PfAMA1 produced in *Nicotiana benthamiana* and analysis of growth inhibitory responses in rabbits. Plant Biotechnol. J. 13, 222–234.
Brochet, X., et al., 2008. IMGT/V-QUEST: the highly customized and integrated system for IG and TR standardized V-J and V-D-J sequence analysis. Nucleic Acids Res. 36.
Cao, J., et al., 2009. Rhoptry neck protein RON2 forms a complex with microneme protein AMA1 in *Plasmodium falciparum* merozoites. Parasitol. Int. 58, 29–35.
Chesne-Seck, M.L., et al., 2005. Structural comparison of Apical Membrane Antigen 1 orthologues and paralogues in apicomplexan parasites. Mol. Biochem. Parasitol. 144, 55–67.
Coley, A.M., et al., 2001. Rapid and precise epitope mapping of monoclonal antibodies against *Plasmodium falciparum* AMA1 by combined phage display of fragments and random peptides. Protein Eng. 4, 691–698.
Coley, A.M., et al., 2006. The most polymorphic residue on *Plasmodium falciparum* Apical Membrane Antigen 1 determines binding of an invasion-inhibitory antibody. Infect. Immun. 74, 2628–2636.
Coley, A.M., et al., 2007. Structure of the malaria antigen AMA1 in complex with a growth-inhibitory antibody. PLoS Pathog. 3, 1308–1319.
Collins, C.R., et al., 2006. Fine mapping of an epitope recognized by an invasion-inhibitory monoclonal antibody on the malaria vaccine candidate Apical Membrane Antigen 1. J. Biol. Chem. 282, 7431–7441.
Cowman, A.F., et al., 2017. The molecular basis of erythrocyte invasion by malaria parasites. Cell Host Microbe. 22, 232–245.
Deans, J.A., et al., 1982. Rat monoclonal antibodies which inhibit the in vitro multiplication of *Plasmodium knowlesi*. Clin. Exp. Immunol. 49, 297–309.
Delgadillo, R.F., et al., 2016. Stability of the *Plasmodium falciparum* AMA1-RON2 complex is governed by the Domain II (DII) loop. PLoS One. 11, e0144764.
Emsley, P., et al., 2010. Features and development of Coot. Acta Crystallogr. D Biol. Crystallogr. 66, 486–501.
Faber, B.W., et al., 2007. Malaria vaccine-related benefits of a single protein comprising *Plasmodium falciparum* Apical Membrane Antigen 1 domains I and II fused to a modified form of the 19-kilodalton C-terminal fragment of merozoite surface protein 1. Infect. Immun. 75, 5947–5955.
Giudicelli, V., et al., 2011. IMGT/V-QUEST: IMGT standardized analysis of the immunoglobulin (IG) and T cell receptor (TR) nucleotide sequences. Cold Spring Harb. Protoc. 2011, 695–715.
Harris, K.S., et al., 2005. Binding hot spot for invasion inhibitory molecules on *Plasmodium falciparum* Apical Membrane Antigen 1. Infect. Immun. 73, 6981–6989.
Henderson, K.A., et al., 2007. Structure of an IgNAR-AMA1 complex: targeting a conserved hydrophobic cleft broadens malarial strain recognition. Structure. 15, 1452–1466.
Hossain, M.E., et al., 2012. The cysteine-rich regions of *Plasmodium falciparum* RON2 bind with host erythrocyte and AMA1 during merozoite invasion. Parasitol. Res. 110, 1711–1721.
Kabsch, W., 2010. XDS. Acta Crystallogr. D Biol. Crystallogr. 66, 125–132.
Kang, S.A., et al., 1991. Combinatorial immunoglobulin libraries in phage λ. Methods: A Companion to Methods in Enzymology 2, pp. 111–118.
Krissinel, E., Henrick, K., 2007. Inference of macromolecular assemblies from crystalline state. J. Mol. Biol. 372, 774–797.
Lamarque, M., et al., 2011. The RON2-AMA1 interaction is a critical step in moving junction-dependent invasion by apicomplexan parasites. PLoS Pathog. 7, e1001276.
Lim, S.S., et al., 2014. Structure and dynamics of apical membrane antigen 1 from *Plasmodium falciparum* FVO. Biochemistry. 53, 7310–7320.
McCoy, A.J., et al., 2007. Phaser Crystallographic Software. J. Appl Crystallogr. 40, 658–674.
Murshudov, G.N., et al., 1997. Refinement of Macromolecular Structures by the Maximum-Likelihood method. Acta Crystallogr. D Biol. Crystallogr. 53, 240–255.
Narum, D.L., Thomas, A.W., 1994. Differential localization of full-length and processed forms of PF83/AMA-1 an apical membrane antigen of *Plasmodium falciparum* merozoites. Mol. Biochem. Parasitol. 67, 59–68.
Pizarro, J.C., et al., 2005. Crystal structure of the malaria vaccine candidate Apical Membrane Antigen 1. Science. 308, 408–411.
Riglar, D.T., et al., 2011. Super-resolution dissection of coordinated events during malaria parasite invasion of the human erythrocyte. Cell Host Microbe. 9, 9–20.
Srinivasan, P., et al., 2011. Binding of *Plasmodium* merozoite proteins RON2 and AMA1 triggers commitment to invasion. Proc. Natl. Acad. Sci. u. s. a. 108, 13275–13280.
Srinivasan, P., et al., 2013. Disrupting malaria parasite AMA1-RON2 interaction with a small molecule prevents erythrocyte invasion. Nat. Commun. 4, 2261.
Vulliez-Le Normand, B., et al., 2004. Expression, crystallization and preliminary structural analysis of the ectoplasmic region of Apical Membrane Antigen 1 from *Plasmodium vivax*, a malaria-vaccine candidate. Acta Crystallogr. D Biol. Crystallogr. 60, 2040–2043.
Vulliez-Le Normand, B., et al., 2012. Structural and functional insights into the malaria parasite moving junction complex. PLoS Pathog. 8, e1002755.
Vulliez-Le Normand, B., et al., 2015. Crystal structure of *Plasmodium knowlesi* Apical Membrane Antigen 1 and its complex with an invasion-inhibitory monoclonal antibody. PLoS One. 10, e0123567.
Vulliez-Le Normand, B., et al., 2017. Cross-reactivity between Apical Membrane Antigen 1 and Rhoptry Neck Protein 2 in *P. vivax* and *P. falciparum*: a structural and binding study. PLoS One. 12, e0183198.
Wang, G., et al., 2016. Structure-Activity Studies of β-Hairpin Peptide Inhibitors of the *Plasmodium falciparum* AMA1-RON2 Interaction. J. Mol. Biol. 428, 3986–3998.
Winn, M.D., et al., 2011. Overview of the CCP4 suite and current developments. Acta Crystallogr. D Biol. Crystallogr. 67, 235–242.